

UNIVERSIDAD SAN FRANCISCO DE QUITO USFQ

Colegio de Posgrados

Spontaneous Scalarization of Einstein–Power–Maxwell systems

**Tesis en torno a una hipótesis o problema
de investigación**

Mikaela Salomé Carrasco Hidalgo

**Ernesto Contreras, Ph.D.
Director de Trabajo de Titulación**

**Carlos Herdeiro, Ph.D.
Codirector de Trabajo de Titulación**

Trabajo de titulación de posgrado presentado como requisito
para la obtención del título de Magíster en Física

Quito, December 16, 2023

UNIVERSIDAD SAN FRANCISCO DE QUITO
USFQ
COLEGIO DE POSGRADOS

HOJA DE APROBACIÓN DE TRABAJO DE TITULACIÓN

Spontaneous Scalarization of Einstein–Power–Maxwell systems

Mikaela Salomé Carrasco Hidalgo

Nombre del Director del Programa: Dario Niebieskikwiat

Título académico: Doctor en Física

Director del programa de: Maestría en Física

Nombre del Decano del Colegio Académico: Eduardo Alba

Título académico: Doctor en Ciencias Matemáticas

Decano del Colegio: Colegio de Ciencias e Ingeniería

Nombre del Decano del Colegio de Posgrados: Hugo Burgos Yáñez

Título académico: Doctorado en Estudios de Medios

Quito, Diciembre 16, 2023

© DERECHOS DE AUTOR

Por medio del presente documento certifico que he leído todas las Políticas y Manuales de la Universidad San Francisco de Quito USFQ, incluyendo la Política de Propiedad Intelectual USFQ, y estoy de acuerdo con su contenido, por lo que los derechos de propiedad intelectual del presente trabajo quedan sujetos a lo dispuesto en esas Políticas.

Asimismo, autorizo a la USFQ para que realice la digitalización y publicación de este trabajo en el repositorio virtual, de conformidad a lo dispuesto en la Ley Orgánica de Educación Superior del Ecuador.

Nombre del Estudiante: Mikaela Salomé Carrasco Hidalgo

Código del Estudiante: 329388

C.I.: 0401867148

Lugar y Fecha: Quito, Diciembre 16, 2023

ACLARACIÓN PARA PUBLICACIÓN

Nota: El presente trabajo, en su totalidad o cualquiera de sus partes, no debe ser considerado como una publicación, incluso a pesar de estar disponible sin restricciones a través de un repositorio institucional. Esta declaración se alinea con las prácticas y recomendaciones presentadas por el Committee on Publication Ethics COPE descritas por Barbour et al. (2017) Discussion document on best practice for issues around theses publishing, disponible en <http://bit.ly/COPETHeses>.

UNPUBLISHED DOCUMENT

Note: The following graduation project is available through Universidad San Francisco de Quito USFQ institutional repository. Nonetheless, this project – in whole or in part – should not be considered a publication. This statement follows the recommendations presented by the Committee on Publication Ethics COPE described by Barbour et al. (2017) Discussion document on best practice for issues around theses publishing available on <http://bit.ly/COPETHeses>.

To the stars in the sky, my grandparents

Acknowledgments

I extend my deepest gratitude to the Gr@v Group at Aveiro University for their warm hospitality and unwavering support throughout the development of this work. Their welcoming environment has greatly contributed to the positive experience of undertaking this research.

Additionally, I wish to express my sincere thanks to the Master in Physics program at USFQ for their generous financial support, which has played a crucial role in the successful completion of this project.

I would like to acknowledge and extend special appreciation to Nuno Santos and Carlos Herdeiro for their invaluable collaboration in the numerical aspects of this research. Their expertise and guidance have significantly enriched the quality and depth of this study.

Finally, I am truly grateful for Ernesto Contrera's commitment to excellence, their insightful feedback, and the time and effort he dedicated to helping me navigate the challenges of this project. His mentorship has not only enriched my academic experience but has also contributed significantly to my personal and professional growth.

My heartfelt thanks to everyone who has been a part of this journey, contributing to the growth and success of this work.

Resumen

Este trabajo explora la escalarización espontánea de agujeros negros soportados por fuentes electromagnéticas. En este marco, el modelo escalar Einstein–Maxwell es revisado, y el modelo Einstein–Power–Maxwell es propuesto. Para este último, mostramos que, para valores particulares de la potencia, surge un agujero negro escalarizado bien comportado, estable y termodinámicamente favorecido, superando al agujero negro libre de escalares.

Palabras clave: escalarización espontánea, agujeros negros, potencia–maxwell, electrodinámica no lineal.

Abstract

This work explore spontaneous scalarization of black holes supported by electromagnetic sources. Within this framework, the Einstein–Maxwell scalar model is reviewed, and the Einstein–Power–Maxwell model is proposed. In the latter, we showed that, for a particular value of the power, a well behaved, stable and thermodynamically favoured scalarized black hole solution emerges, outperforming the scalar–free black hole.

Keywords: spontaneous scalarization, black holes, power–maxwell, non–linear electrodynamics.

Contents

Resumen	7
Abstract	8
1 Introduction	13
2 Spontaneous scalarization of Reissner–Nordström Black Holes	16
2.1 Einstein–Maxwell scalar model	16
2.2 Requirements	19
2.2.1 Asymptotically flat solution	19
2.2.2 Virial Identity	20
2.2.3 Bekenstein–type Identities	24
2.3 Einstein–Maxwell scalar Black Holes solution	25
2.3.1 Specific solution for a scalarized charged Black Hole	25
2.3.2 Bifurcation Diagram for charged Black Holes	26
3 Non–linear electrodynamics and Power–Maxwell	29
3.1 Einstein–Power–Maxwell model	31
3.2 Scalarization of Einstein–Power–Maxwell Black Holes	32
3.2.1 Results and Discussion	35
4 Conclusions	39
References	41

Appendices	48
A Numerical Setup	49
A.1 Particular Solution	50
A.2 Bifurcation Diagram	50
B Analytical solution of the scalar field equation of Reissner–Nordström Black Hole	53
C Mathematical derivation of the virial identity for electromagnetic sources	56
C.1 Virial Identity of Einstein–Maxwell scalar model	56
C.2 Virial Identity of Einstein–Power–Maxwell model	58

List of Figures

2.1	Profile of a scalarized Einstein–Maxwell scalar Black Hole	26
2.2	Domain of existence of scalarized Einstein–Maxwell scalar Black Holes . .	28
2.3	$q = Q/M$ vs. $a_H = \frac{A_H}{16\pi M^2}$ diagram for Einstein–Maxwell scalar model. . .	28
3.1	Profile for scalarized Einstein–Power–Maxwell system with power $3/5$. . .	36
3.2	Mass function for scalarized Einstein–Power–Maxwell system with power $3/5$	37
3.3	Bifurcation diagram for Einstein–Power–Maxwell systems with power $3/5$.	37
3.4	$q = Q/M$ vs. $a_H = \frac{A_H}{16\pi M^2}$ diagram for Einstein–Power–Maxwell systems with power $3/5$	38

List of Tables

3.1	Possible indexes n for Einstein–Power–Maxwell system	34
-----	------------------------------------------------------------------	----

Chapter 1

Introduction

The detection of gravitational waves by LIGO-Virgo-Kagra collaboration [1–7] has ushered in a new era in physics, enabling the exploration of hitherto uncharted areas of gravitational phenomena. These observations enable us to test General Relativity (GR), with Black Holes (BHs) capturing the scientific community’s attention for testing GR in strong gravity regimes. This interest has grown significantly with the breakthroughs in supermassive imaging BH shadows by the Event Horizon Telescope [8–13].

While GR is a well tested theory in the weak field regime, both phenomenological and theoretical factors suggest the need of an extension or modification of the theory. On one hand, GR lacks consistency with the observed accelerated expansion of the universe. On the other hand, it presents various challenges when attempting to unify it with quantum theories. Among several possibilities, in the quest to construct a renormalizable theory it is proposed that the Einstein–Hilbert action should be supplemented with non–linear terms, such as second order curvature invariants non–minimal coupled to dynamical scalar fields [14–17].

In this context, new modified gravity theories have emerged, one of such theories feature a mechanism that is suppressed when gravity is weak. This mechanism initially proposed by Damour and Esposito–Farèse (DEF model) in 1993 [18] to study neutron stars, is known as *spontaneous scalarization* (SS), that resembles a phase transition in which the scalar field needs to adopt a non–trivial configuration when a certain quan-

tity surpasses a threshold. Although, DEF model has been severely constrained by GR tests involving binary pulsars [19–24], SS has gained renewed interest due to the realization that BH solutions of GR can also exhibit scalarization with appropriate scalar field couplings in extended scalar–tensor theories [15, 25–28], Einstein–Maxwell scalar (EMS) models [29] and other novel approaches [30, 31]. These models challenge the ”no–hair” theorem [32] which posits that the only observable properties of a BH should be its mass, charge, and angular momentum.

The hallmark of SS is a tachyonic instability that becomes apparent through linear perturbation in the scalar field, leading to a transition toward a system characterized by non–trivial scalar hair. This instability entails a growth in the scalar field, eventually quenched by non–linear effects in the system. Consequently, the spacetime settles into a stable configuration featuring a BH coupled with scalar hair (also known as hairy BH). Within this framework, one of the most outstanding theories is the extended scalar–tensor Gauss Bonnet model firstly proposed by Doneva and O’ Silva in [15, 25] where scalarized Schwarzschild–like BHs arise under extreme curvature conditions. To understand the latter, let us consider a non–minimal coupling between a massless non–trivial scalar field ϕ , with Schwarzschild Gauss–Bonnet scalar

$$\mathcal{G} = R^2 - 4R_{\mu\nu}R^{\mu\nu} + R_{\mu\nu\alpha\beta}R^{\mu\nu\alpha\beta} = \frac{48M^2}{r^6},$$

where R is the Ricci scalar, $R_{\mu\nu}$ is the Ricci tensor, $R_{\mu\nu\alpha\beta}$ is the Riemann tensor and M is the mass. The dynamics of the scalar field is given by

$$\square\phi + f_{,\phi}(\phi)\mathcal{G} = 0, \tag{1.1}$$

where $f(\phi)$ is the coupling function, $\square = \nabla_\mu\nabla^\mu$ and $f_{,\phi} = df/d\phi$. To satisfy the above equation and ensure the existence of a scalar–free solution when $\phi = 0$, we require that $f_{,\phi}(0) = 0$. Now, the SS occurs when the scalar–free solution is unstable under scalar perturbations $\phi \rightarrow \phi_0 + \delta\phi$ with $\phi_0 = 0$ without loss of generality. In this scenario, the

dynamics obey

$$(\square - \mu_{eff}^2) \delta\phi = 0, \quad (1.2)$$

where $\mu_{eff}^2 = f_{,\phi\phi}(0)\mathcal{G}/4$ is an effective mass acquired by the scalar field with $f_{,\phi\phi} = d^2f/d\phi^2$. Note by that taking $f_{,\phi\phi} < 0$ implies $\mu_{eff}^2 < 0$ so, a tachyonic instability sets in, driving the system away from the scalar-free solution. Additionally, within this model, scalarized BHs are thermodynamically preferred over the vacuum solutions and stable against radial perturbations [33]. In similar vein, Herdeiro and his colleagues presented analogous results in EMS models in [29]. However, in this instance, the SS is triggered by a matter source, akin to the conventional DEF model [18], rather than relying on higher curvature corrections. This EMS model examines electrovacuum BHs, where SS is induced by the Maxwell scalar $F^2 = F_{\mu\nu}F^{\mu\nu}$ serving as an electromagnetic source of matter. Their study demonstrates that, through non-linear numerical simulations, the solution results in a perturbatively stable scalarized BH, which is energetically favoured over the Reissner-Nordström (RN) BH as well.

In recent years, numerous SS models have been investigated (see for instance [16, 34–43]). However, non-linear electrodynamics (NLED) models have not received sufficiently attention. To date, there has been only one study in this regard in [31], which involves a coupling between a scalar field and the Born-Infeld scalar [44, 45]. Given the ongoing research on regular BHs in both four and higher dimensions [46–50], there appears to be a growing need for a more profound understanding of SS in NLED models. In this context, our work presents a new proposal involving a specific class of NLED referred to as the Einstein-Power-Maxwell (EPM) model where the matter source is expressed as an arbitrary power of the Maxwell invariant, namely $(F_{\mu\nu}F^{\mu\nu})^n$ [51, 52]. The organization of this work is as follows. In the next chapter, we examine the EMS model proposed in [29] as it serves as the principal reference for the strategy in solving the Einstein field equations, relevant to the new EPM proposal. Subsequently, in chapter 3 we will delve into the specific details of the SS of EPM systems. Finally, the last chapter, will be dedicated to presenting our final remarks and conclusions.

In this work we shall use geometrical units with $c = 4\pi G = 1$.

Chapter 2

Spontaneous scalarization of Reissner–Nordström Black Holes

In this chapter we will examine SS of RN BHs as initially proposed by Herdeiro and colleagues in Ref. [29] which is a component of EMS models. This chapter is structured as follows. Firstly, we will introduce the proposal along with the equations of motion of the model. Secondly, we will outline the necessary conditions for solving the scalarized system. Finally, we present the results divided in two parts: a specific solution and the bifurcation diagram of scalarized RN BHs.

2.1 Einstein–Maxwell scalar model

Let us start by considering the following action,

$$\mathcal{S} = \frac{1}{4} \int d^4x \sqrt{-g} [R - 2\nabla_\mu \phi \nabla^\mu \phi - f(\phi)\mathcal{I}], \quad (2.1)$$

where R is the Ricci scalar, $\phi = \phi(r)$ is the scalar field, $f(\phi)$ is the coupling function and

$$\mathcal{I} = F_{\mu\nu}F^{\mu\nu}, \quad (2.2)$$

is the electromagnetic source where $F_{\mu\nu}$ is the Maxwell Tensor with a pure electric connection: $A = V(r)dt$.

The generic line element for spherical configuration is

$$ds^2 = -N(r)e^{-2\delta(r)}dt^2 + \frac{dr^2}{N(r)} + r^2d\theta^2 + r^2\sin^2(\theta)d\varphi^2, \quad (2.3)$$

with

$$N(r) = 1 - \frac{2m(r)}{r}, \quad (2.4)$$

where $m(r)$ is the mass function.

The variational principle on the action (2.1) leads in the following field equations

$$\square\phi - f_{,\phi}(\phi)\frac{\mathcal{I}}{4} = 0, \quad (2.5)$$

$$(e^\delta r^2 f(\phi)V')' = 0, \quad (2.6)$$

$$G_{\mu\nu} + g_{\mu\nu}(\nabla\phi)^2 - 2\nabla_\mu\phi\nabla_\nu\phi + \frac{g_{\mu\nu}}{2}f(\phi)\mathcal{I} - 2f(\phi)F_\mu^\sigma F_{\nu\sigma} = 0, \quad (2.7)$$

with $\square = \nabla_\mu\nabla^\mu$. We note that, the dynamics of the scalar field is given by Eq. (2.5) which is trivially satisfied for the scalar-free solution ($\phi = 0$) when $f_{,\phi}(\phi) \propto \phi = 0$. Now, to explore the existence of SS, let us analyze whether the scalar-free solution becomes unstable under perturbation $\phi \rightarrow \phi_0 + \delta\phi$, with $\phi_0 = 0$. Eq. (2.5) becomes,

$$\left(\square - f_{,\phi\phi}(0)\frac{\mathcal{I}}{4}\right)\delta\phi = 0, \quad (2.8)$$

where we identify the effective mass as,

$$\mu_{eff}^2 \equiv f_{,\phi\phi}(0)\frac{\mathcal{I}}{4}. \quad (2.9)$$

Note that, in order to exhibit tachyonic instability we require $f_{,\phi\phi}(0)$ and \mathcal{I} to have opposite sign. In this particular, we have $\mathcal{I} = -2e^{2\delta}V'^2 < 0$, then $f_{,\phi\phi}(0) > 0$. To satisfy the condition, the simplest compatible coupling function that also admits the scalar-free

solution (in contrast to the case of Einstein–Maxwell dilaton [53]) is

$$f(\phi) = e^{-\alpha\phi^2}, \quad (2.10)$$

with α a dimensionless negative constant called *coupling constant*.

Introducing the metric in equations (2.5)–(2.7), we obtain the explicit equations of motion

$$m' = \frac{1}{2}r^2N\phi'^2 + \frac{1}{2}e^{2\delta-\alpha\phi^2}r^2V'^2, \quad (2.11)$$

$$\delta' + r\phi'^2 = 0, \quad (2.12)$$

$$\left(e^{\delta-\alpha\phi^2}r^2V'\right)' = 0, \quad (2.13)$$

$$\left(e^{-\delta}r^2\phi'N\right)' = \alpha e^{\delta-\alpha\phi^2}\phi r^2V'^2. \quad (2.14)$$

From (2.13), we notice the existence of a first integral,

$$V'(r) = -e^{-\delta+\alpha\phi^2}\frac{Q^2}{r^2}, \quad (2.15)$$

where Q is the electric charge.

Given that the equations (2.11)–(2.15) are second order non-linear coupled partial differential equations, their resolution poses a non-trivial challenge. Therefore, it is common practice to employ various numerical techniques with the *shooting method* standing out as the most prevalent choice. This method entails an iterative process wherein initial values for the unknowns are adjusted to meet the prescribed conditions at the boundary. In this model, the functions to be solved numerically, between the event horizon r_H , and infinity, are the mass function, the $\delta(r)$ function and the scalar field. The conditions at infinity are well known as we require an asymptotically flat solution. However, at this stage, the exact values of the functions at r_H are unknown. To reduce the number of

unknowns, we expand the functions in the vicinity of r_H

$$\begin{aligned}
m(r) &= \frac{r_H}{2} + m_1(r - r_H) + \dots \\
\delta(r) &= \delta_0 + \delta_1(r - r_H) + \dots \\
\phi(r) &= \phi_0 + \phi_1(r - r_H) + \dots \\
V(r) &= v_1(r - r_H) + \dots
\end{aligned} \tag{2.16}$$

with

$$\begin{aligned}
\delta_1 &= -\phi_1^2 r_H, \\
v_1 &= -\frac{e^{-\delta_0 + \alpha\phi_0^2}}{r_H^2}, \\
m_1 &= \frac{e^{\alpha\phi_0^2} Q^2}{2r_H^2}, \\
\phi_1 &= \frac{1}{r_H} \frac{\alpha\phi_0 Q^2 e^{\alpha\phi_0^2}}{r_H^2 - Q^2 e^{\alpha\phi_0^2}},
\end{aligned} \tag{2.17}$$

from where we reduced the unknowns to two: δ_0 and ϕ_0 . Furthermore, note that our system remains invariant under $\delta \rightarrow \delta + \tilde{\delta}$, where $\tilde{\delta}$ is a constant, so we can initially set $\delta_0 = 0$. Consequently, we reduce the number of unknown parameters to just one, ϕ_0 , which will serve as the *shooting parameter*. It is worth noticing that, even using the shooting method to reduce the unknowns at the horizon to one, the system has 3 extra degrees of freedom: Q , r_H and α . Therefore, the system continues to be a difficult numerical challenge. Additionally, in order to solve the system, we require specific conditions as we shall see in detail in the next subsection.

2.2 Requirements

2.2.1 Asymptotically flat solution

SS mechanism leads to indistinguishable theories from GR in low curvature regimes. In consequence, as observers at infinity the scalarized solution must be asymptotically flat.

Then, the condition states

$$\begin{aligned}\phi &\rightarrow 0, \\ \delta &\rightarrow 0,\end{aligned}\tag{2.18}$$

and

$$f(0) \rightarrow 1,\tag{2.19}$$

to allow the existence of the scalar-free solution. For a coupling function with an exponential form such as (2.10), the last aforementioned requirement is trivially satisfied. In particular, for this model, we recover the RN solution whose line element is

$$ds^2 = -N(r) + \frac{dr^2}{N(r)} + r^2(d\theta^2 + \sin^2(\theta)d\varphi^2),\tag{2.20}$$

with

$$N(r) = 1 - \frac{2M}{r} + \frac{Q^2}{r^2}.\tag{2.21}$$

2.2.2 Virial Identity

The virial identity is an integral identity used to establish no-go theorems and to verify the accuracy of numerical calculations in non-linear field theories. The construction of the identity follows the classical approach of particle mechanics [54–57]. The virial identity imposed over a system of N bound particles, relates the averages over time of the total kinetic energy T ,

$$\langle T \rangle = -\frac{1}{2} \sum_{i=1}^N \langle \vec{F}_i \cdot \vec{r}_i \rangle,\tag{2.22}$$

where \vec{F}_i is the force of the i^{th} particle in position \vec{r}_i .

Consider a conservative force, $\vec{F} = -\nabla U$ with central potentials like $U(r) = kr^n$. For one particle with $n = -1$ as special case, the virial reads,

$$\langle T \rangle = \frac{1}{2} \left\langle r \frac{\partial U}{\partial r} \right\rangle = \frac{n}{2} \langle U \rangle.\tag{2.23}$$

The previous expression, by definition, can be written in terms of an integral. For periodic motion then,

$$\int_{t_i}^{t_f} \left(T + \frac{U}{2} \right) dt = 0. \quad (2.24)$$

Interestingly, we note that, the previous virial-like identity can be recovered by a *scaling argument* of the classical action,

$$\begin{aligned} S &= \int_{t_i}^{t_f} L dt \\ &= \int_{t_i}^{t_f} (T - U) dt, \end{aligned} \quad (2.25)$$

with T and $U = U(r)$ homogeneous functions of degree 2 and -1 respectively. By considering a rescaling by the factor γ : $\vec{r}(t) \rightarrow \gamma \vec{r}$, the action is

$$S_\gamma = \int_{t_i}^{t_f} (\gamma^2 T - \gamma^{-1} U) dt. \quad (2.26)$$

We notice that, in order to remain stationary at the original solution, the action must obey

$$\left. \frac{\partial S}{\partial \gamma} \right|_{\gamma=1} = 0, \quad (2.27)$$

from where we recover Eq. (2.24).

In the standard variational treatment, we consider an action functional \mathcal{S} that depends on the generalized coordinates q_j with $j = 1, \dots, N$ and its first time derivatives $\dot{q}_j = dq_j/dt$, which is given by

$$\mathcal{S}[q_j(t), \dot{q}_j(t), t] = \int_{t_i}^{t_f} L(q_j, \dot{q}_j, t). \quad (2.28)$$

In addition to the approach described above, the equations of motion can be derived from an *effective action*,

$$\mathcal{S}_{eff} \left[q_j(r), \frac{dq_j(r)}{dr}, r \right] = \int_{r_i}^{\infty} \mathcal{L}_{eff} \left(q_j, \frac{dq_j}{dr}, r \right) dr, \quad (2.29)$$

which extremizes a particular *spacial path*, described by the map

$$\begin{aligned} [r_i, \infty] \in \mathbb{R} &\rightarrow \mathbb{R}^n \\ r &\rightarrow q_j(r). \end{aligned} \tag{2.30}$$

Analogously, we can employ a scale transformation

$$r \rightarrow \tilde{r} = r_i + \lambda(r - r_i), \tag{2.31}$$

where λ is a positive constant which induces a new profile

$$q_j(r) \rightarrow q_j^\lambda(r) = q_j(\tilde{r}). \tag{2.32}$$

Note that, (2.31) scales r but keeps r_i fixed, and the case when $r = \tilde{r}$ is recovered for $\lambda = 1$. Then, the effective action becomes a function of λ ,

$$\begin{aligned} S_{eff}^\lambda &= \int_{r_i}^{\infty} \mathcal{L}_{eff}^\lambda \left(q_j(r), \frac{dq_j(r)}{dr}, r \right) dr, \\ &= \int_{r_i}^{\infty} \mathcal{L}_{eff} \left(q_j(\tilde{r}), \frac{dq_j(\tilde{r})}{d\tilde{r}}, \tilde{r} \right) d\tilde{r}, \\ &= \int_{r_i}^{\infty} \mathcal{L}_{eff} \left(q_j(\tilde{r}), \lambda \frac{dq_j(\tilde{r})}{d\tilde{r}}, \tilde{r} \right) \frac{d\tilde{r}}{\lambda}, \end{aligned}$$

from where the stationary condition follows,

$$\left. \frac{\partial S_{eff}^\lambda}{\partial \lambda} \right|_{\lambda=1} = 0. \tag{2.33}$$

The Eq. (2.33) leads to the original equations of motion of the standard variational principle as long as

$$\int_{r_i}^{\infty} \left[\sum_j \frac{\partial \mathcal{L}_{eff}}{\partial q_j'} q_j' - \mathcal{L}_{eff} - \frac{\partial \mathcal{L}_{eff}}{\partial r} (r - r_i) \right] dr = 0. \tag{2.34}$$

is satisfied.

In this work, we face particular problems where the effective Lagrangian can be written

as

$$\mathcal{L}'_{eff}(q_j, q'_j, r) = \mathcal{L}_{eff}(q_j, q'_j, r) + \frac{d}{dr}f(q_j, q'_j, r), \quad (2.35)$$

where the contribution of the total derivative df/dr does not affect the equations of motion.

Even though, the treatment is developed for systems with finite degrees of freedom, this strategy can be directly extended to fields. As an illustrative example of GR, let us consider the following parametrization

$$ds^2 = -\sigma^2(r) \left(1 - \frac{2m(r)}{r}\right) dt^2 + \left(1 - \frac{2m(r)}{r}\right)^{-1} dr^2 + r^2 d\Omega^2,$$

that allows us to write the effective Einstein–Hilbert action

$$\begin{aligned} \mathcal{S}_{eff} &= \int \mathcal{L}'_{eff}(\sigma, m; \sigma' m'; r) dr \\ &= \int \sigma r^2 R dr \\ &= \int 4\sigma m' dr + \int \frac{d}{dr} [2\sigma' r(2m - r) + 2\sigma(m'r - m)] dr \end{aligned}$$

from where we recognize,

$$f(\sigma, m; \sigma' m'; r) = 2\sigma' r(2m - r) + 2\sigma(m'r - m).$$

Then, the effective lagrangian for this particular expression is just

$$\mathcal{L}_{eff}(\sigma, m; \sigma' m'; r) = 4\sigma m'.$$

Now, by considering the full RN action (2.1) with electromagnetic source (2.2) and metric (2.3), the effective Lagrangian takes the form

$$\mathcal{L}_{eff} = e^{-\delta} m' - \frac{1}{2} e^{-\delta} r^2 N \phi'^2 + \frac{1}{2} e^{\delta - \alpha \phi^2} r^2 V'^2. \quad (2.36)$$

Notice that when using the effective Lagrangian (2.36), the Euler–Lagrange equations

yield the same equations of motion obtained through variational principle, as given in equations (2.11)–(2.14).

Now, by assuming (2.36) and the existence of an event horizon, $r_H = r_i$, the virial-like identity explicitly reads (for details see Appendix C),

$$\int_{r_H}^{\infty} dr \left\{ e^{-\delta} r^2 \phi'^2 \left[1 + \frac{2r_H}{r} \left(\frac{m}{r} - 1 \right) \right] \right\} = \int_{r_H}^{\infty} dr \left[e^{-\delta - \alpha \phi^2} \left(1 - \frac{2r_H}{r} \right) \frac{Q^2}{r^2} \right]. \quad (2.37)$$

This virial-like provides insights into the constrains on our system. In particular, the charge must be non-zero, as the left hand side of the above expression consistently remains non-negative. Therefore, it establishes a no-go theorem regarding the charge to admit the existence of scalarized charged BH. Additionally, the identity serves as a tool to verify the numerical accuracy of the results. To achieve this, the virial-like identity is rearranged to make it equal to zero. Typically, a numerical solution is considered well-behaved, if it yields a value less than 10^{-4} .

2.2.3 Bekenstein-type Identities

Bekenstein-type identities impose certain constrains on the scalarized solutions through the integration of the scalar field equation (2.5) and multiplication by specific factors. Following Brihaye and others in Ref. [58], we present two examples:

1. Multiplying Eq. (2.5) by $f_{,\phi}$ and after integrating by parts and using the divergence theorem, we get,

$$\int_V d^4x \sqrt{-g} \left[f_{,\phi\phi} (\nabla\phi)^2 + f_{,\phi}^2 \frac{\mathcal{I}}{4} \right] = 0, \quad (2.38)$$

from where we require $f_{,\phi\phi}$ and \mathcal{I} to have opposite sign.

2. Multiplying Eq. (2.5) by ϕ , we get

$$\int_V d^4x \sqrt{-g} \left[(\nabla\phi)^2 + \phi f_{,\phi} \frac{\mathcal{I}}{4} \right] = 0. \quad (2.39)$$

from where we require $\phi f_{,\phi}$ and \mathcal{I} to have opposite sign.

In particular, for scalarized RN BH with (2.2) and (2.10) we need $f_{,\phi\phi}$ and $\phi f_{,\phi}$ to be positive for all $\alpha < 0$.

Now, with all the requirements in place, we will reproduce the main results of Herdeiro and others [29] in the next section.

2.3 Einstein–Maxwell scalar Black Holes solution

At this point, we would like to remark that, the objective is to solve the system (2.11)–(2.15) for any $r_H < r < \infty$, where the boundary conditions are fixed by (2.16), and by the requirement in subsection 2.2.1. Since, we are considering a coupling function such as (2.10) with $\alpha < 0$, the requirement 2.2.3 is trivially satisfied while the virial identity specified in 2.2.2 holds for any $Q \neq 0$.

With the aforementioned pieces in place, we are now equipped to solve the system. The results of a specific solution is presented in the following subsection 2.3.1. Subsequently, in subsection 2.3.2 we explore the domain of existence where a family of scalarized solutions bifurcates from the scalar–free solution.

2.3.1 Specific solution for a scalarized charged Black Hole

The system of equations (2.11)–(2.15) must be solved for the scalar field, the mass function and the metric function $\delta(r)$ numerically (see Appendix A for details). In figure 2.1 we present the results for the scalarized RN BH, for parameters $\alpha = -2$, $Q = 0.45$ and $M = 0.4454$. Note that, as in Ref. [29], all the profiles exhibit well behaved characteristics. Specifically, $\phi(r)$ and $\delta(r)$ are monotonically decreasing functions that asymptotically approach zero as $r \rightarrow \infty$. Furthermore, $m(r)$ reaches a maximum value, M , which coincides with the RN mass value. Lastly, as expected from equation (2.15), the expression $-r^2V'(r)$ converges to the value Q .

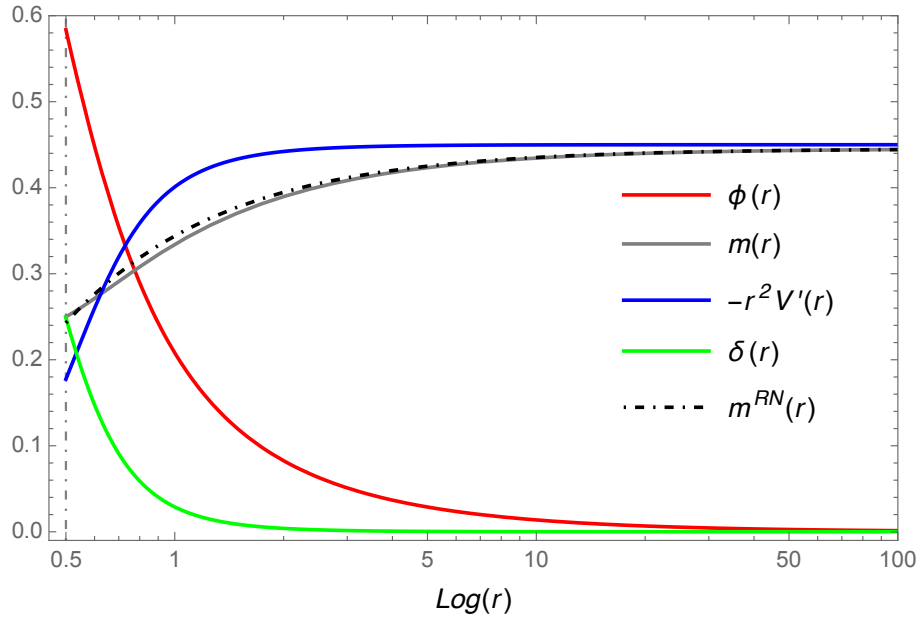


Figure 2.1: Profile of a scalarized RN BH (solid lines) with $\alpha = -2$, $Q = 0.45$ and $M = 0.4454$ and, mass function for free RN BH (dot-dashed line) for same Q and M .

2.3.2 Bifurcation Diagram for charged Black Holes

The bifurcation diagram is a graphical representation within a parameter space where a deviation of scalarized BHs from the scalar-free solution is shown. It is bounded by the *existence line* and a *critical set* (orange and blue line in Fig. 2.2 respectively). The first denotes the points at which scalarized solutions bifurcate from RN BHs, while the second involves physical considerations fixed depending on the model of study, as we shall see. Between these two bounds there is the *domain of existence* which refers to the region where we can find a family of scalarized solutions.

For finding the existence line, let us consider a spherical harmonics decomposition of the scalar field as

$$\delta\phi(r, \theta, \varphi) = \sum_{\ell m} Y_{\ell m} U_{\ell}(r), \quad (2.40)$$

from where the perturbed scalar field equation (2.8) becomes,

$$\frac{e^{\delta}}{r^2} \frac{d}{dr} \left(\frac{r^2 N}{e^{\delta}} \frac{dU_{\ell}}{dr} \right) - \left[\frac{\ell(\ell+1)}{r^2} + \mu_{eff}^2 \right] U_{\ell} = 0. \quad (2.41)$$

The above expression represents an eigenvalue problem for particular values of ℓ . Since we require an asymptotically vanishing scalar field, a discrete set of BHs can be obtained

which correspond to the *bifurcation points* of the RN solution.

For spherical symmetric system $\ell = 0$, we find the exact solution for (2.41),

$$U_0(r) = P_u \left[1 + \frac{2Q^2(r - r_H)}{r(r_H^2 - Q^2)} \right], \quad (2.42)$$

where

$$u = \frac{-1 + \sqrt{4\alpha + 1}}{2}, \quad (2.43)$$

$$r_H = M + \sqrt{M^2 - Q^2}, \quad (2.44)$$

and P_u is a Legendre function (the steps for finding U_0 are detailed in Appendix B).

Since $\phi(r) = 0$ as $r \rightarrow \infty$, the task of identifying the bifurcation points is reduced to study the zeros of U_0 in the limit of infinity. Consequently, the expression is simplified to generic parameters (α, Q, r_H) and it becomes feasible to obtain the existence line for any $\alpha < -1/4$.

For finding the domain of existence, one implements a numerical recurrence by fixing Q , α and varying r_H . For each r_H , the equations of motion (2.11)-(2.14) are solved, and the initial guess for ϕ_0 is the real value obtained from the shooting method of the previous solution. Each α -branch ends at the numerical defined critical set determined by the divergence of the temperature and vanishing area at the horizon. The whole domain of existence is depicted in Fig. 2.2 (See Appendix A for numerical details). In the domain of existence, there exist a region of nonuniqueness ($q < 1$) in which scalarized and scalar-free BHs coexist. For this region, the scalarized solutions prove to be entropically favoured over the RN BHs, see Fig.2.3.

It is worth noticing that, for the family of scalarized solutions in the domain of existence, the virial identity yielded a value of $\sim 10^{-5}$. Therefore, all the solutions exhibit good numerical behavior.

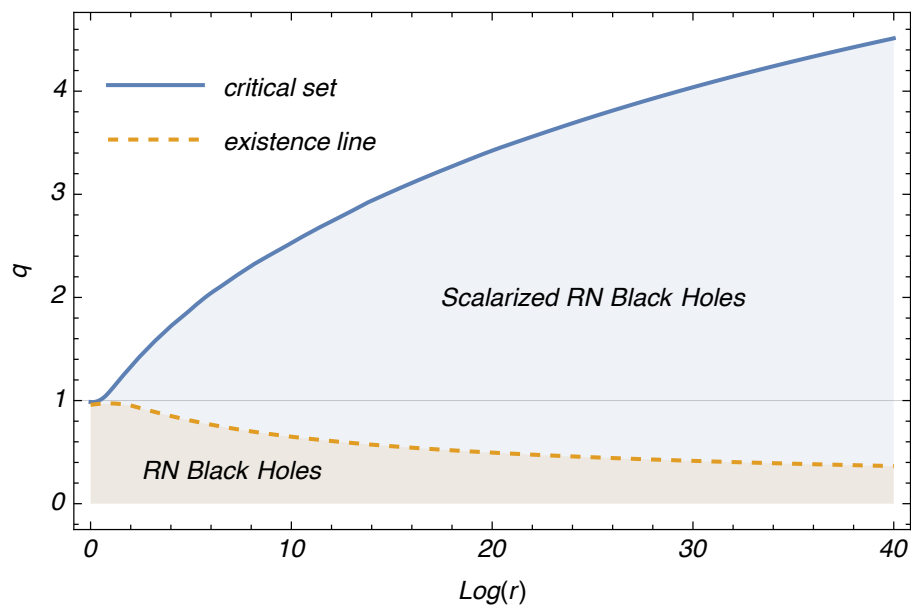
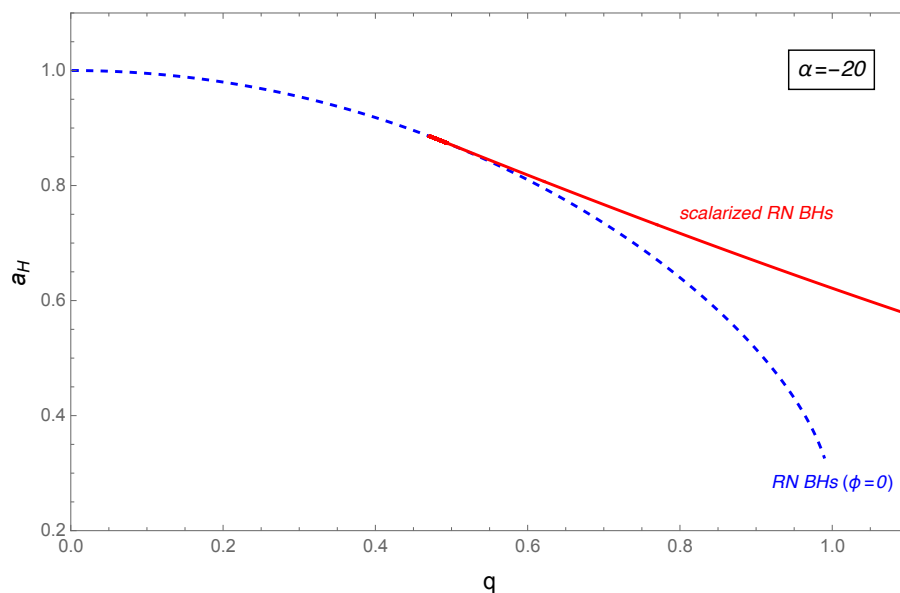


Figure 2.2: Domain of existence of scalarized EM BHs.

Figure 2.3: $q = Q/M$ vs. $a_H = \frac{A_H}{16\pi M^2}$ diagram where A_H is the horizon area for scalarized (solid line) and scalar-free (dashed line) EMS BHs at $\alpha = -20$.

Chapter 3

Non-linear electrodynamics and Power-Maxwell

The motivation behind NLED, initially proposed by Born and Infeld in 1934, [45], is twofold. Firstly, it addresses the issue that the self-energy of a point charge is infinite in classical electrodynamics. Secondly, the theory aims to unify quantum mechanics with electrodynamics. To tackle the first issue, it is necessary to impose an upper bound, b , on the energy. Consequently, the Lagrangian of Maxwell's theory

$$\mathcal{L} = -\frac{1}{4}F_{\mu\nu}F^{\mu\nu} = -\frac{1}{2}(E^2 - B^2),$$

has to be replaced by

$$\mathcal{L} = b^2 \left(1 - \sqrt{1 - \frac{E^2 - B^2}{b^2} - \frac{(\vec{E} \cdot \vec{B})^2}{b^4}} \right).$$

This replacement is akin to the idea of special relativity where $\frac{1}{2}mv^2$ is substituted by the relativistic expression $mc^2 \left(1 - \sqrt{1 - \frac{v^2}{c^2}} \right)$, reflecting the limitation of particle velocities by the speed of light, c .

Although this new field theory failed in unifying with quantum mechanics, the Born-Infeld theory has found extensions to a wide array of models. These include its in-

corporation into string theory [59, 60], gravitational theories for modeling regular BHs [46–50, 61, 62], applications in cosmology tackling problems such as inflation or dark energy [63–65], implications in condensed matter [66] and other contexts [67, 68]. These models of NLED encompass a variety of functional forms, including logarithmic, double-logarithmic, exponential, rational, arcsin, power-law, inverse and others [69].

Despite its extensive applications in various physical problems, NLED has not been thoroughly explored in the context of SS. As far as we know, there is only one study in this domain, as presented in [31] involving a coupling between the scalar field and the Born–Infeld scalar [44, 45]. Nevertheless, we believe that further research on SS in NLED is compulsory. One specific class arises from the generalization of the Born–Infeld model: the power Maxwell model, in which the matter source is determined by a Lagrangian expressed as an arbitrary power of the Maxwell invariant, namely

$$\mathcal{L} \sim (F_{\mu\nu}F^{\mu\nu})^n$$

[51, 52]. It is worth noting that when the power of the absolute value of the Maxwell scalar is set to be $d/4$ (where d represents the spacetime dimension), the power–Maxwell action exhibits conformal invariance. However, this conformal invariance is not upheld in higher dimensions, despite the RN solution maintaining it in four dimensions. In light of this, in [52] the authors introduce a relaxation of the conformal condition by considering an arbitrary power of the Maxwell scalar. Within their research, they demonstrate that for power values of n greater than $1/2$ or less than 0 , the scalar curvature displays a singularity at the origin. Conversely, for values of n ranging from 0 to $1/2$, the scalar curvature diverges at infinity. Notably, when n falls within the range of $(1/2, 3/2)$ with a rational number with an odd denominator, the solution exhibits behavior akin to the standard RN solution in the sense that the charge contribution in the metric decreases more rapidly than the mass contribution. In this chapter, we study the SS on an EPM system for a particular value of the power n within the range of $(1/2, 3/2)$.

3.1 Einstein–Power–Maxwell model

Let us consider the same action as in (2.1), namely,

$$\mathcal{S} = \frac{1}{4} \int d^4x \sqrt{-g} [R - 2\nabla_\mu \phi \nabla^\mu \phi - f(\phi)\mathcal{I}], \quad (3.1)$$

where in this case, the electromagnetic source \mathcal{I} is given by

$$\mathcal{I} = (F_{\mu\nu}F^{\mu\nu})^n \quad (3.2)$$

with $F = dA$ as the usual Maxwell tensor with an electric gauge connection only (i.e. $A = V(r)dt$) and n a positive constant.

Again, the line element is the same as (2.3):

$$ds^2 = -N(r)e^{-2\delta(r)}dt^2 + \frac{dr^2}{N(r)} + r^2d\theta^2 + r^2\sin^2(\theta)d\varphi^2, \quad (3.3)$$

with

$$N(r) = 1 - \frac{2m(r)}{r}. \quad (3.4)$$

The equations of motion of the system can be obtained either through the variational principle, or by utilizing the following effective Lagrangian

$$\mathcal{L}_{eff} = e^{-\delta}m' - \frac{1}{2}e^{-\delta}r^2N\phi'^2 - 2^{n-2}r^2e^{-\delta}f(\phi)(-e^{2\delta}V'^2)^n. \quad (3.5)$$

from where, the explicit equations of motion are

$$m' = \frac{1}{2}r^2N\phi'^2 - 2^{n-2}(2n-1)r^2f(\phi)(-e^{2\delta}V'^2)^n, \quad (3.6)$$

$$\delta' + r\phi'^2 = 0, \quad (3.7)$$

$$\left[e^\delta f(\phi)r^2n(-2e^{2\delta}V'^2)^{n-1}V' \right]' = 0, \quad (3.8)$$

$$(e^{-\delta}r^2\phi'N)' = 2^{n-2}r^2f_{,\phi}(\phi)e^{-\delta}(-e^{2\delta}V'^2)^n. \quad (3.9)$$

The integration of (3.8) is straightforward leading to,

$$V'(r) = e^{-\delta} \left[\frac{(-1)^n Q}{2^{n-1} n r^2 f(\phi)} \right]^{\frac{1}{2n-1}}, \quad (3.10)$$

where Q is the electric charge. Note that, as expected, when $n \rightarrow 1$, the aforementioned equations simplify to (2.11)-(2.15) corresponding to the scalarized RN BHs as discussed in the previous chapter.

Now, we aim to identify the necessary ingredients for scalarization of EPM systems. To achieve this, we will adopt the same strategy as outlined in section 2.2 of the preceding chapter. Once we have the conditions in place, we can proceed to solve the system. All the steps involved in this process are elaborated upon in the next section.

3.2 Scalarization of Einstein–Power–Maxwell Black Holes

As previously discussed, SS arise when the system is ‘tachyonical’ unstable under perturbations of the scalar field. In this case, the dynamics of the scalar field obeys

$$\nabla^\mu \nabla_\mu \phi - f_{,\phi}(\phi) \frac{(F_{\mu\nu} F^{\mu\nu})^n}{4} = 0. \quad (3.11)$$

If we perturb the scalar field in the form of $\phi \rightarrow \phi_0 + \delta\phi$ with $\phi_0 = 0$, the above expression is reduced to,

$$\left[\square - f_{,\phi\phi}(0) \frac{(F_{\mu\nu} F^{\mu\nu})^n}{4} \right] \delta\phi = 0, \quad (3.12)$$

from where we identify the effective mass in the background as,

$$\mu_{eff}^2 \equiv f_{,\phi\phi}(0) \frac{(F_{\mu\nu} F^{\mu\nu})^n}{4}. \quad (3.13)$$

Then, to promote the system to SS, it is required a negative effective mass, which requires that $f_{,\phi\phi}(0)$ and $\mathcal{I} = (F_{\mu\nu} F^{\mu\nu})^n$ to have opposite signs. In particular, for the

parametrization (3.3), the electromagnetic source is

$$\mathcal{I} = (-2e^{2\delta}V'^2)^n, \quad (3.14)$$

from where we note a dependence of \mathcal{I} in the particular values of n . To analyze the allowed values of n , let us study the virial identity for this model (see Appendix C for details). By using the general expression (2.34) with $r_i = r_H$ and the effective Lagrangian (3.5), we obtain

$$\int_{r_H}^{\infty} dr \left\{ e^{-\delta} r^2 \phi'^2 \left[1 + \frac{2r_H}{r} \left(\frac{m}{r} - 1 \right) \right] \right\} = \quad (3.15)$$

$$- \frac{1}{2} \int_{r_H}^{\infty} dr \left\{ r^2 e^{-\delta} f(\phi) (-2e^{2\delta}V'^2)^n \left(3 - 2n - \frac{2r_H}{r} \right) \right\}.$$

Since the left hand side of (3.15) is consistently positive, we must confine ourselves to non-zero charges and specific values of n , in order to ensure that the right hand side of (3.15) remains positive as well. Two particular cases arise. On one hand, we have $n > 1$ satisfying $(-1)^n > 0$. On the other hand, $n \leq 1$ but it must satisfy $(-1)^n < 0$. To determine an specific value of n let us take a closer look at the classical solution. Following [52, 70], the scalar-free line element can be written as

$$ds^2 = - \left(1 + \frac{C}{r} + \frac{B}{r^\beta} \right) dt^2 + \left(1 + \frac{C}{r} + \frac{B}{r^\beta} \right)^{-1} dr^2 + r^2 (d\theta^2 + \sin^2(\theta)d\varphi^2), \quad (3.16)$$

where $C = -2M$,

$$B = - \frac{4(-1)^n (2Q^2)^n (2n - 1)^2}{2(3 - 2n)}, \quad (3.17)$$

and

$$\beta = \frac{2}{2n - 1}. \quad (3.18)$$

It is worth noticing that, although β could be arbitrary, the simplest choice is to consider it as a natural number in which case n must take the values shown in Table 3.1.

Notably, there are two viable options for n that correspond to the cases where $n \leq 1$ with $(-1)^n < 0$. The first option is $n = 1$, but this case essentially recovers the RN BH

β	n	β	n
1	3/2	6	2/3
2	1	7	9/14
3	5/6	8	5/8
4	3/4	9	11/18
5	7/10	10	3/5

Table 3.1: Corresponding values of n for the first ten values of β .

that was covered by Herdeiro in Ref.[29], as detailed in chapter 2. The second choice which satisfies the virial condition is $n = \frac{3}{5}$. Therefore, we will focus our attention on this specific choice.

Thus, for the SS of a system triggered by an electromagnetic source such as (3.14) with $n = \frac{3}{5}$, the system must meet the following requirements:

1. *Tachyonic Instability.* Given that $\mathcal{I} < 0$, to guarantee that the effective mass (3.13) is negative, we demand $f_{,\phi\phi}(0)$ to be positive.
2. *Asymptotically flat solution.* To ensure the recovery of the scalar-free solution at infinity, the scalarized solution must adhere to the condition of asymptotic flatness which requires $\phi \rightarrow 0$, $f(\phi \rightarrow 0) = 1$, $\delta \rightarrow 0$ and

$$N(r) = 1 - \frac{2M}{r} + 2\frac{(2Q^2)^{3/5}}{45r^{10}}, \quad (3.19)$$

as $r \rightarrow \infty$.

3. *Bekenstein-type identities.* This condition requires both $f_{,\phi\phi}$ and $\phi f_{,\phi}$ to be positive.

Once more, the simplest coupling function that trivially fulfill all of the aforementioned requirements is

$$f(\phi) = e^{-\alpha\phi^2}, \quad (3.20)$$

with $\alpha < 0$.

The coupling function (3.20) and the previous requirements allows us to solve the system (3.6)–(3.9) for any $r_H < r < \infty$. The results are presented in the following subsection.

3.2.1 Results and Discussion

As in the SS of the RN BH, the system must be solved for the scalar field, the mass function and the $\delta(r)$ function. Due to the asymptotically flat requirement, the conditions of the functions at infinity are well known but, once again their values at r_H are unknown. Then, one finds the approximate solutions to the equations of motion,

$$\begin{aligned}
 m(r) &= \frac{r_H}{2} + m_1(r - r_H) + \dots \\
 \delta(r) &= \delta_0 + \delta_1(r - r_H) + \dots \\
 \phi(r) &= \phi_0 + \phi_1(r - r_H) + \dots \\
 V(r) &= v_1(r - r_H) + \dots
 \end{aligned} \tag{3.21}$$

with

$$\begin{aligned}
 \delta_1 &= -\phi_1^2 r_H, \\
 v_1 &= e^{-\delta_0} \left[\frac{(-1)^n Q}{2^{n-1} n r_H^2 f(\phi_0)} \right]^{\frac{1}{2n-1}}, \\
 m_1 &= -2^{n-2} (2n-1) r_H^2 f(\phi_0) \left[\frac{(-1)^n Q}{2^{n-1} n r_H^2 f(\phi_0)} \right]^{\frac{2n}{2n-1}}, \\
 \phi_1 &= \frac{(-1)^n 2^{n-2} n r_H f_{,\phi}(\phi_0)}{n + (2n-1) Q \left[\frac{(-1)^n Q}{2^{n-1} n r_H^2 f(\phi_0)} \right]^{\frac{1}{2n-1}}} \left[\frac{(-1)^n Q}{2^{n-1} n r_H^2 f(\phi_0)} \right]^{\frac{2n}{2n-1}},
 \end{aligned} \tag{3.22}$$

from where we recognize δ_0 and ϕ_0 as the unknowns of the system. Similar to SS of RN BH, this system remains invariant under $\delta \rightarrow \delta + \tilde{\delta}$ with $\tilde{\delta}$ constant. As a result, $\delta_0 = 0$ and we are left with just ϕ_0 as the sole unknown parameter to be determined using the shooting method.

For the numerical solution, we identify the degrees of freedom of the system as Q , r_H , α and the initial guess of ϕ_0 (numerical details can be found in Appendix A). Figures 3.1 and 3.2 present the results for a particular solution for the specific values in the legend. The scalar field and δ are depicted as functions of r , both remaining regular and positive at the horizon and decreasing monotonously as $r \rightarrow \infty$. The function $-r^{10}V'$ is also shown, converging to a constant determined by the expression in (3.10). Finally, in Fig.

3.2 the mass function for the scalarized and scalar-free BHs are displayed, with both functions converging to the expected constant M .

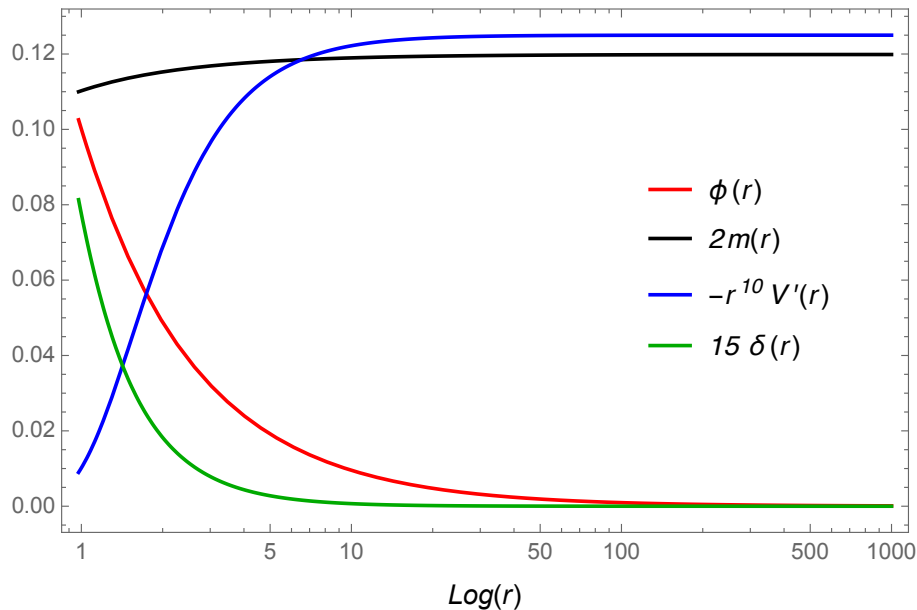


Figure 3.1: Profile for scalarized EPM system for $Q = 0.3$, $\alpha = -50$ and $r_H = 0.1$.

Now, in order to construct the bifurcation diagram, we will follow the same strategy as for the RN model. Firstly, to obtain the existence line (orange dashed line in Fig. 3.3), we will employ the same spherical harmonics decomposition of the scalar field

$$\phi(r, \theta, \varphi) = \sum_{\ell m} Y_{\ell m}(\theta, \varphi) U_{\ell}(r), \quad (3.23)$$

by substituting the previous expression in the scalar field equation (3.12) from where we obtain

$$\frac{e^{\delta}}{r^2} \frac{d}{dr} \left(\frac{r^2 N}{e^{\delta}} \frac{dU_{\ell}}{dr} \right) - \left[\frac{\ell(\ell+1)}{r^2} + \mu_{eff}^2 \right] U_{\ell} = 0, \quad (3.24)$$

where N is the scalar-free function (3.19) of the metric (3.3). For the spherical symmetric case, $\ell = 0$, identifying the bifurcation points involves studying the zeros of the solution for U_0 . However, Eq. (3.24) lacks an analytical solution for U_0 so we implement a numerical technique in which we select the value of $q = Q/M$ for which U_0 has roots closest to zero (see Appendix A for details). In consequence, we will obtain the first bifurcation points in the background of the EPM system.

Secondly, the upper bound of the domain of existence (blue line in Fig. 3.3) can be

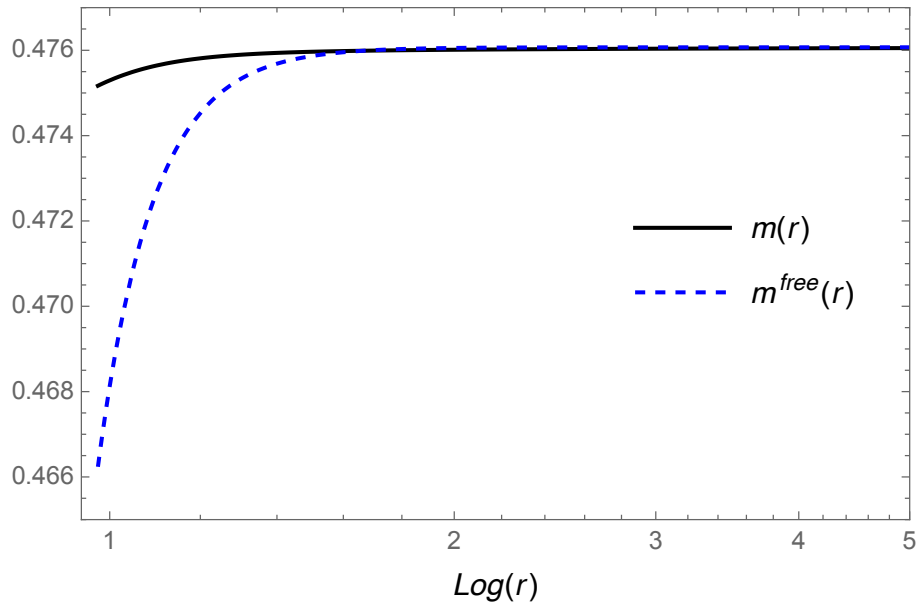


Figure 3.2: Mass function for scalarized and scalar-free EPM BH with $Q = 0.3$, $\alpha = -50$, $r_H^{\phi \neq 0} = 0.95$ and $r_H^{\phi = 0} = 0.9177$.

obtained through the usual numerical recurrence fixing Q and α and varying r_H . Each α -branch ends at the numerical critical set determined by the area at the horizon (which approaches to zero). The entire solution is depicted in Fig. 3.3.

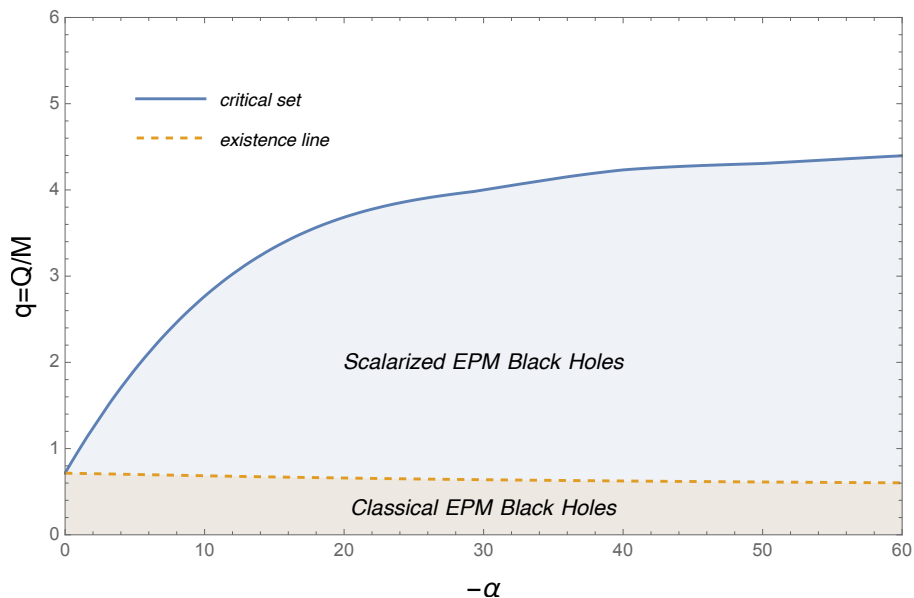


Figure 3.3: Bifurcation diagram for EPM systems with power $3/5$.

Note that, as in the previous case, there exists a nonuniqueness region in the domain of existence where scalar-free and the scalarized BHs coexist defined by the values of q for which the metric N has real roots. In such a region, the scalarized solutions are

entropically preferred as shown in Fig. 3.4 for the specific values in the legend.

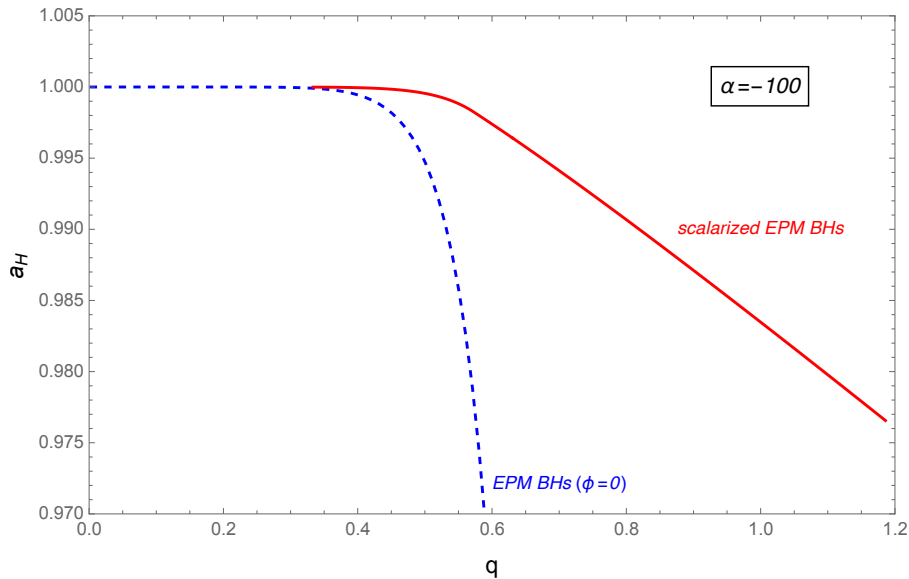


Figure 3.4: $q = Q/M$ vs. $a_H = \frac{A_H}{16\pi M^2}$ diagram where A_H is the horizon area for scalarized (solid line) and scalar-free (dashed line) EPM BHs at $\alpha = -100$.

Let us summarize the main results. The equations of motion were solved throughout demanding numerical calculations. To minimize the difficulty of this task we implemented the shooting method over the parameter ϕ_0 , while the other (model-dependent) free parameters, Q , α and r_H were given by hand. By implementing recurrence steps, it was possible to construct a particular solution (Fig. 3.1) and the bifurcation diagram (Fig. 3.3). Both behaviours are particularly similar to the case of SS of RN BHs [29]. Furthermore, there exist a region of coexistence (at $\sim q = 0.6$ in Fig. 2.3) between the scalar-free and scalarized BHs. In this region, the scalarized BH has a bigger horizon area which implies a bigger entropy. Therefore, the scalarized BHs are thermodynamically favoured over the scalar-free state. Furthermore, all the scalarized solutions are well-behaved, exhibiting values of approximate 10^{-6} for the virial identity.

Chapter 4

Conclusions

In this work, we investigated the spontaneous scalarization supported by a non-linear electrodynamic source non-minimally coupled to a scalar field. Our primary focus was on proposing an scalarized Einstein–Power–Maxwell model $\mathcal{L} \propto (F_{\mu\nu}F^{\mu\nu})^n$, a generalization of the previously introduced scalarized Einstein–Maxwell scalar model and scalarized Born–Infeld model in [29] and [31], respectively.

For a coupling function with an exponential form $e^{-\alpha\phi^2}$ with $\alpha < 0$, our solutions satisfied all the conditions. Namely, a negative effective mass, the asymptotically flatness condition, the Bekenstein–type identities and the virial identity. Our findings revealed that, based on the virial identity, the power of the Maxwell scalar cannot take any arbitrary value but it must be constrained in a very specific way in order to ensure scalarization. We specifically focused on the case where $n < 1$ and set the power in a way that the free solution corresponds to a straightforward modification of the Reissner–Nordström metric, namely, a metric containing $r^{-\beta}$ with $\beta \in \mathbb{N}$. Our analysis indicated that the scalarized solution is entropically favored compared to its hairless counterpart, aligning with observations for the scalarized Reissner–Nordström black hole.

It could be interesting to explore arbitrary (n, l, m) scalar clouds and to study the stability of the solution against perturbations, similar to the analysis in [29]. Additionally, given the golden era for testing strong gravity, a further comparison of the phenomenology of scalarized Einstein–Power–Maxwell systems with current data could be intriguing.

However, these and other aspects lie out of the scope of the present work and we leave them for future developments. Finally, to improve the efficiency in the numerical calculations, we suggest the use of a cluster.

Bibliography

- [1] R. Abbott et al. Search for continuous gravitational wave emission from the milky way center in o3 ligo-virgo data. *Phys. Rev. D*, 106:042003, Aug 2022.
- [2] R. Abbott et al. Search for gravitational waves from scorpius x-1 with a hidden markov model in o3 ligo data. *Phys. Rev. D*, 106:062002, Sep 2022.
- [3] R. Abbott et al. All-sky search for continuous gravitational waves from isolated neutron stars using advanced ligo and advanced virgo o3 data. *Phys. Rev. D*, 106:102008, Nov 2022.
- [4] R. Abbott et al. All-sky search for gravitational wave emission from scalar boson clouds around spinning black holes in ligo o3 data. *Phys. Rev. D*, 105:102001, May 2022.
- [5] R. Abbott et al. All-sky, all-frequency directional search for persistent gravitational waves from advanced ligo's and advanced virgo's first three observing runs. *Phys. Rev. D*, 105:122001, Jun 2022.
- [6] R. Abbott et al. Search for subsolar-mass binaries in the first half of advanced ligo's and advanced virgo's third observing run. *Phys. Rev. Lett.*, 129:061104, Aug 2022.
- [7] R. Abbott et al. Search for continuous gravitational waves from 20 accreting millisecond x-ray pulsars in o3 ligo data. *Phys. Rev. D*, 105:022002, Jan 2022.
- [8] Kazunori Akiyama et al. First M87 Event Horizon Telescope Results. I. The Shadow of the Supermassive Black Hole. *Astrophys. J. Lett.*, 875:L1, 2019.

-
- [9] Kazunori Akiyama et al. First M87 Event Horizon Telescope Results. VI. The Shadow and Mass of the Central Black Hole. *Astrophys. J. Lett.*, 875(1):L6, 2019.
- [10] Kazunori Akiyama et al. First M87 Event Horizon Telescope Results. III. Data Processing and Calibration. *Astrophys. J. Lett.*, 875(1):L3, 2019.
- [11] Kazunori Akiyama et al. First M87 Event Horizon Telescope Results. V. Physical Origin of the Asymmetric Ring. *Astrophys. J. Lett.*, 875(1):L5, 2019.
- [12] Kazunori Akiyama et al. First M87 Event Horizon Telescope Results. I. The Shadow of the Supermassive Black Hole. *Astrophys. J. Lett.*, 875:L1, 2019.
- [13] Kazunori Akiyama et al. First M87 Event Horizon Telescope Results. II. Array and Instrumentation. *Astrophys. J. Lett.*, 875(1):L2, 2019.
- [14] K. S. Stelle. Renormalization of Higher Derivative Quantum Gravity. *Phys. Rev. D*, 16:953–969, 1977.
- [15] Daniela D. Doneva and Stoytcho S. Yazadjiev. New Gauss-Bonnet Black Holes with Curvature-Induced Scalarization in Extended Scalar-Tensor Theories. *Phys. Rev. Lett.*, 120(13):131103, 2018.
- [16] Hao-Jui Kuan, Alan Tsz-Lok Lam, Daniela D. Doneva, Stoytcho S. Yazadjiev, Masaru Shibata, and Kenta Kiuchi. Dynamical scalarization during neutron star mergers in scalar-Gauss-Bonnet theory. *Phys. Rev. D*, 108(6):063033, 2023.
- [17] Emanuele Berti et al. Testing General Relativity with Present and Future Astrophysical Observations. *Class. Quant. Grav.*, 32:243001, 2015.
- [18] Thibault Damour and Gilles Esposito-Farèse. Nonperturbative strong-field effects in tensor-scalar theories of gravitation. *Phys. Rev. Lett.*, 70:2220–2223, Apr 1993.
- [19] Paulo C. C. Freire, Norbert Wex, Gilles Esposito-Farèse, Joris P. W. Verbiest, Matthew Bailes, Bryan A. Jacoby, Michael Kramer, Ingrid H. Stairs, John Antoniadis, and Gemma H. Janssen. The relativistic pulsar-white dwarf binary PSR

- J1738+0333 II. The most stringent test of scalar-tensor gravity. *Mon. Not. Roy. Astron. Soc.*, 423:3328, 2012.
- [20] Lijing Shao, Noah Sennett, Alessandra Buonanno, Michael Kramer, and Norbert Wex. Constraining nonperturbative strong-field effects in scalar-tensor gravity by combining pulsar timing and laser-interferometer gravitational-wave detectors. *Phys. Rev. X*, 7(4):041025, 2017.
- [21] David Anderson, Paulo Freire, and Nicolás Yunes. Binary pulsar constraints on massless scalar–tensor theories using Bayesian statistics. *Class. Quant. Grav.*, 36(22):225009, 2019.
- [22] John Antoniadis, Paulo C. C. Freire, Norbert Wex, et al. A massive pulsar in a compact relativistic binary. *Science*, 340(6131):1233232, 2013.
- [23] M. Kramer et al. Strong-Field Gravity Tests with the Double Pulsar. *Phys. Rev. X*, 11(4):041050, 2021.
- [24] Junjie Zhao, Paulo C. C. Freire, Michael Kramer, Lijing Shao, and Norbert Wex. Closing a spontaneous-scalarization window with binary pulsars. *Class. Quant. Grav.*, 39(11):11LT01, 2022.
- [25] Hector O. Silva, Jeremy Sakstein, Leonardo Gualtieri, Thomas P. Sotiriou, and Emanuele Berti. Spontaneous scalarization of black holes and compact stars from a Gauss-Bonnet coupling. *Phys. Rev. Lett.*, 120(13):131104, 2018.
- [26] Daniela D. Doneva, Lucas G. Collodel, and Stoytcho S. Yazadjiev. Spontaneous nonlinear scalarization of Kerr black holes. *Phys. Rev. D*, 106(10):104027, 2022.
- [27] Pedro V. P. Cunha, Carlos A. R. Herdeiro, and Eugen Radu. Spontaneously Scalarized Kerr Black Holes in Extended Scalar-Tensor–Gauss-Bonnet Gravity. *Phys. Rev. Lett.*, 123(1):011101, 2019.
- [28] Masato Minamitsuji and Taishi Ikeda. Scalarized black holes in the presence of the coupling to Gauss-Bonnet gravity. *Phys. Rev. D*, 99(4):044017, 2019.

-
- [29] Carlos A. R. Herdeiro, Eugen Radu, Nicolas Sanchis-Gual, and José A. Font. Spontaneous Scalarization of Charged Black Holes. *Phys. Rev. Lett.*, 121(10):101102, 2018.
- [30] Georgios Antoniou, Lorenzo Bordin, and Thomas P. Sotiriou. Compact object scalarization with general relativity as a cosmic attractor. *Phys. Rev. D*, 103(2):024012, 2021.
- [31] Peng Wang, Houwen Wu, and Haitang Yang. Scalarized Einstein-Born-Infeld black holes. *Phys. Rev. D*, 103(10):104012, 2021.
- [32] Remo Ruffini and John A. Wheeler. Introducing the black hole. *Phys. Today*, 24(1):30, 1971.
- [33] Jose Luis Blázquez-Salcedo, Daniela D. Doneva, Jutta Kunz, and Stoytcho S. Yazadjiev. Radial perturbations of the scalarized Einstein-Gauss-Bonnet black holes. *Phys. Rev. D*, 98(8):084011, 2018.
- [34] Georgios Antoniou. New perspectives on scalar fields in strong gravity. Other thesis, 8 2023.
- [35] Tamara Evstafyeva, Roxana Rosca-Mead, Ulrich Sperhake, and Bernd Bruggmann. Boson stars in massless and massive scalar-tensor gravity. 10 2023.
- [36] Guangzhou Guo, Peng Wang, Houwen Wu, and Haitang Yang. Scalarized Kerr-Newman black holes. *JHEP*, 10:076, 2023.
- [37] Alexandre M. Pombo, João M. S. Oliveira, and Nuno M. Santos. Coupled scalar-Proca soliton stars. *Phys. Rev. D*, 108(4):044044, 2023.
- [38] Sizheng Ma, Vijay Varma, Leo C. Stein, Francois Foucart, Matthew D. Duez, Lawrence E. Kidder, Harald P. Pfeiffer, and Mark A. Scheel. Numerical simulations of black hole-neutron star mergers in scalar-tensor gravity. *Phys. Rev. D*, 107(12):124051, 2023.

-
- [39] Jie Jiang and Jia Tan. Spontaneous scalarization of dyonic black hole in Einstein–Maxwell-scalar theory. *Eur. Phys. J. C*, 83(4):290, 2023.
- [40] Fahimeh Rahimi and Zeinab Rezaei. Spontaneous scalarization in proto-neutron stars. *Eur. Phys. J. C*, 83(4):289, 2023.
- [41] Ekrem S. Demirboğa, Yakup Emre Şahin, and Fethi M. Ramazanoğlu. Subtleties in constraining gravity theories with mass-radius data. *Phys. Rev. D*, 108(2):024028, 2023.
- [42] Takami Kuroda and Masaru Shibata. Spontaneous scalarization as a new core-collapse supernova mechanism and its multimessenger signals. *Phys. Rev. D*, 107(10):103025, 2023.
- [43] Hengyu Xu and Shao-Jun Zhang. Tachyonic instability of Reissner-Nordström-Melvin black holes in Einstein-Maxwell-scalar theory. *Nucl. Phys. B*, 987:116110, 2023.
- [44] M. Born. Modified field equations with a finite radius of the electron. *Nature*, 132(3329):282.1, 1933.
- [45] M. Born and L. Infeld. Foundations of the new field theory. *Proc. Roy. Soc. Lond. A*, 144(852):425–451, 1934.
- [46] Kirill A. Bronnikov. Regular magnetic black holes and monopoles from nonlinear electrodynamics. *Phys. Rev. D*, 63:044005, 2001.
- [47] Leonardo Balart and Elias C. Vagenas. Regular black holes with a nonlinear electrodynamics source. *Phys. Rev. D*, 90(12):124045, 2014.
- [48] Irina Dymnikova and Evgeny Galaktionov. Regular rotating electrically charged black holes and solitons in non-linear electrodynamics minimally coupled to gravity. *Class. Quant. Grav.*, 32(16):165015, 2015.

- [49] Manuel E. Rodrigues, Edinaldo L. B. Junior, and Marcos V. de Sousa Silva. Using dominant and weak energy conditions for build new classe of regular black holes. *JCAP*, 02:059, 2018.
- [50] K. A. Bronnikov. Nonlinear electrodynamics, regular black holes and wormholes. *Int. J. Mod. Phys. D*, 27(06):1841005, 2018.
- [51] Mokhtar Hassaine and Cristian Martinez. Higher-dimensional black holes with a conformally invariant Maxwell source. *Phys. Rev. D*, 75:027502, 2007.
- [52] Mokhtar Hassaine and Cristian Martinez. Higher-dimensional charged black holes solutions with a nonlinear electrodynamics source. *Class. Quant. Grav.*, 25:195023, 2008.
- [53] David Garfinkle, Gary T. Horowitz, and Andrew Strominger. Charged black holes in string theory. *Phys. Rev. D*, 43:3140, 1991. [Erratum: *Phys.Rev.D* 45, 3888 (1992)].
- [54] Carlos A. R. Herdeiro, João M. S. Oliveira, Alexandre M. Pombo, and Eugen Radu. Virial identities in relativistic gravity: 1d effective actions and the role of boundary terms. *Phys. Rev. D*, 104:104051, Nov 2021.
- [55] M Heusler and N Straumann. Scaling arguments for the existence of static, spherically symmetric solutions of self-gravitating systems. *Classical and Quantum Gravity*, 9(9):2177, sep 1992.
- [56] Markus Heusler. No-hair theorems and black holes with hair, 1996.
- [57] Carlos A. R. Herdeiro and Eugen Radu. Asymptotically flat black holes with scalar hair: A review. *International Journal of Modern Physics D*, 24(9), 2015.
- [58] Yves Brihaye, Carlos Herdeiro, and Eugen Radu. Black Hole Spontaneous Scalarisation with a Positive Cosmological Constant. *Phys. Lett. B*, 802:135269, 2020.
- [59] E.S. Fradkin and A.A. Tseytlin. Non-linear electrodynamics from quantized strings. *Physics Letters B*, 163(1):123–130, 1985.

-
- [60] G. W. Gibbons. Aspects of born-infeld theory and string/m-theory. In *AIP Conference Proceedings*. AIP, 2001.
- [61] G. Abbas, H. Rehman, Tao Zhu, Qiang Wu, and G. Mustafa. Accretion disk around Reissner-Nordström black hole coupled with a nonlinear electrodynamics field. 10 2023.
- [62] S. I. Kruglov. Dyonic and magnetic black holes with rational nonlinear electrodynamics. 1 2023.
- [63] H. B. Benaoum, Luz Ángela García, and Leonardo Castañeda. Early dark energy induced by non-linear electrodynamics. 7 2023.
- [64] Yisong Yang. Nonlinear Problems Inspired by the Born–Infeld Theory of Electrodynamics. 4 2023.
- [65] M. Novello, Santiago Esteban Perez Bergliaffa, and J. Salim. Non-linear electrodynamics and the acceleration of the universe. *Phys. Rev. D*, 69:127301, 2004.
- [66] Vasil Rokač. *Condensed Matter Systems in Cavity Quantum Electrodynamics*. PhD thesis, Universität Hamburg, 2021.
- [67] S.I. Kruglov. A model of nonlinear electrodynamics. *Annals of Physics*, 353:299–306, 2015.
- [68] Igor Bandos, Kurt Lechner, Dmitri Sorokin, and Paul K. Townsend. A non-linear duality-invariant conformal extension of Maxwell’s equations. *Phys. Rev. D*, 102:121703, 2020.
- [69] Dmitri P. Sorokin. Introductory Notes on Non-linear Electrodynamics and its Applications. *Fortsch. Phys.*, 70(7-8):2200092, 2022.
- [70] Ángel Rincón, Ernesto Contreras, Pedro Bargueño, Benjamin Koch, and Grigoris Panotopoulos. Four dimensional Einstein-power-Maxwell black hole solutions in scale-dependent gravity. *Phys. Dark Univ.*, 31:100783, 2021.

Appendices

Appendix A

Numerical Setup

In the context of GR, solving the equations of motion is a primary objective, often tackled using numerical methods. The shooting method is a common technique, particularly for challenging problems, as is the case in this work.

For the problems covered here, the functions requiring numerical solutions within the range $r_H < r < \infty$ include the mass function, the scalar field and the metric function $\delta(r)$. It is necessary to set the boundary conditions at infinity and at the event horizon. Guided by the requirement of asymptotic flatness, the conditions at infinity are well defined, while the values of the functions at the horizon remain unknown. To reduce the number of unknowns, one states an expansion of the functions around the horizon and look at symmetries. In consequence, it becomes feasible to reduce the unknown parameters to one, ϕ_0 (the scalar field at the horizon), which will serve as the *shooting parameter*. Note that, this method requires an *initial guess* value for ϕ_0 which must be close to its real value, in order to find a well behaved solution. From now on, we will denote the initial guess (input) as $\tilde{\phi}_0$ and the real value (output) as ϕ_0 . It is important to highlight that, there exist other model-dependent free parameters that need to be provided manually. In the models examined in this work, these include the charge, the coupling constant, the radius of the horizon and $\tilde{\phi}_0$ as the free parameters. Setting this parameters poses a challenge, as each parameter has only one value for which a scalarized solution is obtained.

This chapter is dedicated to elucidating the particularities of the numerical calculation for scalarized asymptotically flat systems. It is divided into two sections. The first section outlines the numerical implementation for solving a specific solution, while the second section is centered around the construction of the bifurcation diagram.

A.1 Particular Solution

To address the numerical problem, we implemented a defined function, denoted as \mathcal{F} which receives the input parameters of the problem $(Q, \alpha, \delta_0, r_H, \phi_0, r_f)$. Here, r_f represents the final point of integration, essentially infinity. The function contains the expansion around the horizon, the equations of motion and the specific method for solving the partial differential equations. The function returns a value, R which is crucial for the application of the shooting method. This value is determined for the boundary condition of the scalar field at the horizon. By defining $R = (r\phi)'$ as $\phi = 0$ when $r \rightarrow \infty$, it implies that $R = 0$. Therefore, when fixing the charge, the coupling constant and the horizon radius, and varying $\tilde{\phi}_0$, the shooting method aims to find a *numerically stable solution* by driving R towards zero. Numerical stability is achieved when $\tilde{\phi}_0 = \phi_0$.

For practical implementation, we utilized *Wolfram Mathematica*. The equations of motion were solved using the `NDSolve` function with `ExplicitRungeKutta` as the chosen method. To find ϕ_0 , `FindRoot` was employed, specifying $\mathcal{F} = 0$ which means $R = 0$. Notable, we found that, the models investigated in this work are not r_f dependent, and for our purposes, we fixed $r_f = 1000$.

A.2 Bifurcation Diagram

The bifurcation diagram is bounded by two key components: the existence line serving as the lower bound, and the domain of existence with the critical set acting as the upper bound. The initial segment represents the first bifurcation points departing from the scalar-free solution, whereas the latter segment corresponds to the family of scalarized solutions. Both parts are constructed through numerical computation. However, in

certain special models such as the one in Ref. [29], the existence line can be computed in a semi-analytical manner (previously elucidated in subsection 2.3.2).

On one hand, in constructing of the existence line, we initiate the process by introducing a small perturbation of the scalar field, $\delta\phi$ in the background of the scalar-free solution. For spherically symmetric system, we propose a spherical harmonic decomposition of $\delta\phi$. Then, replacing it into the scalar field equation, we derive an ordinary differential equation for a radial function, $U(r)$. As the perturbation tends to zero while we approach the infinity, $U(r)$ maintains the same behaviour, indicating its depending solely on the free parameters, such as $q = Q/M$ and α . Therefore, for finding the first bifurcation point at a fixed α , we must vary q until determining its value for which $U(r \rightarrow \infty)$ approaches zero most closely. The main difference between the semi-analytical procedure and the complete numerical treatment is that the first uses directly the expression of U_0 to find its roots for fixed α , while in the latter, one has to solve the differential equation at each step in the variation of q . In both approaches, the variation of q can be implemented through a **For Loop**. In the full numerical treatment, it is recommended to create another function similar to \mathcal{F} for solving the differential equation for U_0 and apply the shooting method for the condition of U_0 at the horizon. Note that, after implementing the code for a fixed α , we should vary this parameter in small steps and repeat the process as well.

On the other hand, when building the domain of existence and the critical set, a complete numerical calculation is employed. For this process, we shall work around a particular solution that needs to be initially obtained. Each point in the bifurcation diagram over the domain of existence corresponds to one scalarized solution linked to specific values of the free parameters. In the models addressed in this work, the bifurcation diagrams are depicted as α vs. $q = Q/M$ diagrams. It is noteworthy that, M is proportional to r_H . By fixing α and Q while varying r_H , a ‘vertical line’ is obtained in the diagram. For each point on the vertical line, the equations of motion are solved following the same procedure explained in the previous section A.1. Additionally, the value of $\tilde{\phi}_0$ needs to be specified at each step. As the shooting method demands the closest value of $\tilde{\phi}_0$ to ϕ_0 , a form of *recursion* is implemented for this parameter where ϕ_0 from the previous

solution is utilized as the input $\tilde{\phi}_0$ for finding the new solution. Once a line is obtained, α is varied and the process repeated. The critical set is defined by numerical parameters. For scalarized EPM systems the area at the horizon tends to zero and for the scalarized EMS systems in [29] it was shown that the temperature of the horizon diverges and the area at the horizon vanishes.

It is important to highlight that, as we approach the critical set, the steps in r_H are reduced to the order of (at least) 10^{-5} due to the requirements of the shooting method. Essentially, there is a maximum solution beyond which ϕ_0 cannot serve as the input $\tilde{\phi}_0$ for the next solution because these two are too separated from one another. Consequently, the shooting method does not return a numerically stable solution. Therefore, to avoid this problem, it becomes necessary to decrease the space between the two solutions, indicating a reduction in the steps in r_H . Note that, to circumvent this issue, using a cluster where the steps in r_H are sufficiently small from the beginning, could be a viable approach.

Appendix B

Analytical solution of the scalar field equation of Reissner–Nordström Black Hole

This chapter provides the step-by-step guide for obtaining the analytical solution of the ordinary differential equation (ODE) for $U_0(r)$:

$$\frac{1}{r^2} \frac{d}{dr} \left(r^2 N \frac{dU_0}{dr} \right) - \mu_{eff}^2 U_0 = 0. \quad (\text{B.1})$$

with

$$N(r) = 1 - \frac{2M}{r} + \frac{Q^2}{r^2}, \quad (\text{B.2})$$

and

$$\mu_{eff}^2 = \alpha \frac{Q^2}{r^4}, \quad (\text{B.3})$$

which correspond to the free-scalar solution of RN BH. Expanding (B.1) we get

$$\left(-\frac{r^4}{Q^2} + \frac{2Mr^3}{Q^2} - r^2 \right) \frac{d^2 U_0}{dr^2} - 2 \left(\frac{r^3}{Q^2} - \frac{r^2 M}{Q^2} \right) \frac{dU_0}{dr} + \alpha U_0 = 0. \quad (\text{B.4})$$

Given that $U_0(r)$ represents the radial component resulting from the scalar field decomposition, it is reasonable to seek a solution in the form of a Legendre Polynomial.

Then, the ODE for Legendre Polynomials can be seen like

$$(1 - x^2) \frac{d^2 y}{dx^2} - 2x \frac{dy}{dx} + u(u + 1)y = 0, \quad (\text{B.5})$$

where its solution is the Legendre Polynomial:

$$P_u(x). \quad (\text{B.6})$$

Now, we would like to make (B.4) formally the same as (B.5), hence, we propose

$$U_0(r) = \xi(f(r)). \quad (\text{B.7})$$

Substituting U_0 in (B.1) and grouping terms, we get,

$$\begin{aligned} \left(-\frac{r^4}{Q^2} + \frac{2Mr^3}{Q^2} - r^2 \right) \left(\frac{df}{dr} \right)^2 \frac{d^2 \xi}{df^2} + \left[\left(-\frac{r^4}{Q^2} + \frac{2Mr^3}{Q^2} - r^2 \right) \frac{d^2 f}{dr^2} \right. \\ \left. - 2 \left(\frac{r^3}{Q^2} - \frac{r^2 M}{Q^2} \right) \frac{df}{dr} \right] \frac{d\xi}{df} + \alpha \xi = 0. \end{aligned} \quad (\text{B.8})$$

Comparing (B.8) with (B.5) we recognize that $\xi = y$, $f = x$ and

$$u = \frac{\sqrt{4\alpha + 1} - 1}{2}, \quad (\text{B.9})$$

$$1 - f^2 = \left(-\frac{r^4}{Q^2} + \frac{2Mr^3}{Q^2} - r^2 \right) \left(\frac{df}{dr} \right)^2, \quad (\text{B.10})$$

$$-2f = \left(-\frac{r^4}{Q^2} + \frac{2Mr^3}{Q^2} - r^2 \right) \frac{d^2 f}{dr^2} - 2 \left(\frac{r^3}{Q^2} - \frac{r^2 M}{Q^2} \right) \frac{df}{dr}. \quad (\text{B.11})$$

Then, we propose a polynomial form of f

$$f(r) = A + Br^n, \quad (\text{B.12})$$

where A and B are constants. After replacing the proposal in the differential equations

and solving for $n = 1$, we found

$$f(r) = 1 + \frac{2Q^2}{r_H^2 - Q^2} - \frac{2Q^2 r_H}{r(r_H^2 - Q^2)}, \quad (\text{B.13})$$

where

$$r_H = M + \sqrt{M^2 - Q^2}, \quad (\text{B.14})$$

is the RN horizon. Finally, the solution for (B.1) can be expressed in terms of a Legendre Polynomial as

$$U_0(r) = P_u \left[1 + \frac{2Q^2(r - r_H)}{r(r_H^2 - Q^2)} \right]. \quad (\text{B.15})$$

Appendix C

Mathematical derivation of the virial identity for electromagnetic sources

This chapter explores the step-by-step guide for obtaining the virial identities for scalarized systems supported by electromagnetic matter sources: the Maxwell invariant and the power-Maxwell invariant.

The virial identity (in general), for scalarized BHs, with an event horizon r_H , triggered by electromagnetic sources, is given by

$$\int_{r_H}^{\infty} \left[\sum_j \frac{\partial \mathcal{L}_{eff}}{\partial q'_j} q'_j - \mathcal{L}_{eff} - \frac{\partial \mathcal{L}_{eff}}{\partial r} (r - r_H) \right] dr = 0. \quad (\text{C.1})$$

C.1 Virial Identity of Einstein–Maxwell scalar model

For an EMS model, with electromagnetic source (2.2) and metric (2.3), the effective Lagrangian is given by

$$\mathcal{L}_{eff} = e^{-\delta} m' - \frac{1}{2} e^{-\delta} r^2 N \phi'^2 + \frac{1}{2} e^{\delta - \alpha \phi^2} r^2 V'^2. \quad (\text{C.2})$$

Then, the virial identity (C.1) becomes

$$\begin{aligned}
0 &= \int_{r_H}^{\infty} \left[\sum_j \frac{\partial \mathcal{L}_{eff}}{\partial q'_j} q'_j - \mathcal{L}_{eff} - \frac{\partial \mathcal{L}_{eff}}{\partial r} (r - r_H) \right] dr \\
&= \int_{r_H}^{\infty} \left[\cancel{e^{-\delta} m'} - \cancel{e^{-\delta} r^2 N \phi'^2} + \cancel{e^{\delta - \alpha \phi^2} r^2 V'^2} - \cancel{e^{-\delta} m'} + \frac{1}{2} e^{-\delta} r^2 N \phi'^2 - \frac{1}{2} e^{\delta - \alpha \phi^2} r^2 V'^2 \right] dr \\
&+ \int_{r_H}^{\infty} \left[\cancel{e^{-\delta} r^2 N \phi'^2} - e^{-\delta} r r_H N \phi'^2 + \frac{1}{2} e^{-\delta} r^2 N' \phi'^2 (r - r_H) - \cancel{e^{\delta - \alpha \phi^2} r^2 V'^2} + e^{\delta - \alpha \phi^2} r r_H V'^2 \right] dr \\
&= \int_{r_H}^{\infty} \left[\frac{1}{2} e^{-\delta} r^2 N \phi'^2 - \frac{1}{2} e^{\delta - \alpha \phi^2} r^2 V'^2 - e^{-\delta} r r_H N \phi'^2 + \frac{1}{2} e^{-\delta} r^2 N' \phi'^2 (r - r_H) + e^{\delta - \alpha \phi^2} r r_H V'^2 \right] dr,
\end{aligned}$$

but

$$\begin{aligned}
N &= 1 - \frac{2m}{r}, \\
N' &= \frac{\partial N}{\partial r} = \frac{2m}{r^2}, \\
V'^2 &= e^{-2\delta + 2\alpha \phi^2} \frac{Q^2}{r^4}.
\end{aligned}$$

Replacing

$$\begin{aligned}
0 &= \int_{r_H}^{\infty} \left[\frac{1}{2} e^{-\delta} r^2 \phi'^2 - \frac{1}{2} e^{-\delta} r^2 \frac{2m}{r} \phi'^2 - \frac{1}{2} e^{\delta - \alpha \phi^2} r^2 e^{-2\delta + 2\alpha \phi^2} \frac{Q^2}{r^4} \right] dr \\
&+ \int_{r_H}^{\infty} \left[-e^{-\delta} r r_H \phi'^2 + e^{-\delta} r r_H \frac{2m}{r} \phi'^2 + \frac{1}{2} e^{-\delta} r^2 \frac{2m}{r^2} \phi'^2 (r - r_H) + e^{\delta - \alpha \phi^2} r r_H e^{-2\delta + 2\alpha \phi^2} \frac{Q^2}{r^4} \right] dr \\
&= \int_{r_H}^{\infty} \left[\frac{1}{2} e^{-\delta} r^2 \phi'^2 - e^{-\delta} m r \phi'^2 - \frac{1}{2} e^{-\delta + \alpha \phi^2} \frac{Q^2}{r^2} - e^{-\delta} r r_H \phi'^2 + e^{-\delta} 2m r_H \phi'^2 \right] dr \\
&+ \int_{r_H}^{\infty} \left[e^{-\delta} m r \phi'^2 - e^{-\delta} m r_H \phi'^2 + e^{-\delta + \alpha \phi^2} r_H \frac{Q^2}{r^3} \right] dr.
\end{aligned}$$

Rearranging terms

$$\begin{aligned}
0 &= \int_{r_H}^{\infty} \left[\frac{1}{2} e^{-\delta} r^2 \phi'^2 \left(1 - \cancel{\frac{2m}{r}} - \frac{2r_H}{r} + \frac{4m r_H}{r^2} + \cancel{\frac{2m}{r}} - \frac{2m r_H}{r^2} \right) \right] dr \\
&+ \int_{r_H}^{\infty} \left[-\frac{1}{2} e^{-\delta + \alpha \phi^2} \frac{Q^2}{r^2} \left(1 - \frac{2r_H}{r} \right) \right] dr.
\end{aligned}$$

Finally, we obtain

$$\int_{r_H}^{\infty} \frac{1}{2} e^{-\delta} r^2 \phi'^2 \left[1 + \frac{2r_H}{r} \left(\frac{m}{r} - 1 \right) \right] dr = \int_{r_H}^{\infty} \left[\frac{1}{2} e^{-\delta + \alpha \phi^2} \frac{Q^2}{r^2} \left(1 - \frac{2r_H}{r} \right) \right] dr$$

C.2 Virial Identity of Einstein–Power–Maxwell model

For an EPM system, with metric (3.3) and source (3.14), the effective lagrangian takes the form

$$\mathcal{L}_{eff} = e^{-\delta} m' - \frac{1}{2} e^{-\delta} r^2 N \phi'^2 - \frac{1}{4} r^2 e^{-\delta} f(\phi) (-2e^{2\delta} V'^2)^n. \quad (\text{C.3})$$

Similarly to the previous section, by replacing the lagrangian in (C.1) we have

$$\begin{aligned} 0 &= \int_{r_H}^{\infty} \left[\cancel{e^{-\delta} m'} - \cancel{e^{-\delta} r^2 N \phi'^2} - \frac{n}{2} r^2 e^{-\delta} f(\phi) (-2e^{2\delta} V'^2)^n - \cancel{e^{-\delta} m'} + \frac{1}{2} e^{-\delta} r^2 N \phi'^2 \right] dr \\ &+ \int_{r_H}^{\infty} \left[\frac{1}{4} r^2 e^{-\delta} f(\phi) (-2e^{2\delta} V'^2)^n + \cancel{e^{-\delta} r^2 N \phi'^2} - e^{-\delta} r r_H N \phi'^2 \right] dr \\ &+ \int_{r_H}^{\infty} \left[\frac{1}{2} e^{-\delta} r^3 N' \phi'^2 (r - r_H) + \frac{1}{2} r e^{-\delta} f(\phi) (-2e^{2\delta} V'^2)^n (r - r_H) \right] dr, \end{aligned}$$

Rearranging

$$\begin{aligned} 0 &= \int_{r_H}^{\infty} \left[r^2 e^{-\delta} f(\phi) (-2e^{2\delta} V'^2)^n \left(-\frac{n}{2} + \frac{1}{4} + \frac{1}{2} - \frac{r_H}{2r} \right) \right] dr \\ &+ \int_{r_H}^{\infty} \frac{1}{2} e^{-\delta} r^2 \phi'^2 \left[N - 2N \frac{r_H}{r} + N'(r - r_H) \right] dr \\ 0 &= \int_{r_H}^{\infty} \frac{1}{4} r^2 e^{-\delta} f(\phi) (-2e^{2\delta} V'^2)^n \left(3 - 2n - \frac{2r_H}{r} \right) dr \\ &+ \int_{r_H}^{\infty} \frac{1}{2} e^{-\delta} r^2 \phi'^2 \left[1 - \cancel{\frac{2m'}{r}} - \frac{2r_H}{r} + \frac{4mr_H}{r^2} + \cancel{\frac{2m'}{r}} - \frac{2mr_H}{r} \right] dr. \end{aligned}$$

Finally,

$$\begin{aligned} \int_{r_H}^{\infty} dr \left\{ e^{-\delta} r^2 \phi'^2 \left[1 + \frac{2r_H}{r} \left(\frac{m}{r} - 1 \right) \right] \right\} = \\ - \frac{1}{2} \int_{r_H}^{\infty} dr \left\{ r^2 e^{-\delta} f(\phi) (-2e^{2\delta} V'^2)^n \left(3 - 2n - \frac{2r_H}{r} \right) \right\}. \end{aligned} \quad (\text{C.4})$$